PNAS RESEARCH ARTICLE | IMMUNOLOGY AND INFLAMMATION OPEN ACCESS

A distinct human cell type expressing MHCII and RORγt with dual characteristics of dendritic cells and type 3 innate lymphoid cells

Alina Ulezko Antonova[a,1], Silvia Lonardi[b,1], Matilde Monti[b], Francesco Missale[b,c], Changxu Fan[d], Matthew L. Coates[e,f], Mattia Bugatti[b], Natalia Jaeger[a], Patrick Fernandes Rodrigues[a], Simone Brioschi[a], Tihana Trsan[a], José L. Fachi[a], Khai M. Nguyen[a], Ryan M. Nunley[g], Daniele Moratto[h], Stefania Zini[b], Lingjia Kong[i,j,k], Jacques Deguine[j], Mark E. Peeples[l,m,n], Ramnik J. Xavier[i,j,k,o,p], Menna R. Clatworthy[e,q], Ting Wang[d], Marina Cella[a], William Vermi[a,b,2], and Marco Colonna[a,2]

Contributed by Marco Colonna; received October 27, 2023; accepted November 14, 2023; reviewed by Franca Ronchese and Jianhua Yu

Recent studies have characterized various mouse antigen-presenting cells (APCs) expressing the lymphoid-lineage transcription factor RORγt (Retinoid-related orphan receptor gamma t), which exhibit distinct phenotypic features and are implicated in the induction of peripheral regulatory T cells (Tregs) and immune tolerance to microbiota and self-antigens. These APCs encompass Janus cells and Thetis cell subsets, some of which express the AutoImmune REgulator (AIRE). RORγt$^+$ MHCII$^+$ type 3 innate lymphoid cells (ILC3) have also been implicated in the instruction of microbiota-specific Tregs. While RORγt$^+$ APCs have been actively investigated in mice, the identity and function of these cell subsets in humans remain elusive. Herein, we identify a rare subset of RORγt$^+$ cells with dendritic cell (DC) features through integrated single-cell RNA sequencing and single-cell ATAC sequencing. These cells, which we term RORγt$^+$ DC-like cells (R-DC-like), exhibit DC morphology, express the MHC class II machinery, and are distinct from all previously reported DC and ILC3 subsets, but share transcriptional and epigenetic similarities with DC2 and ILC3. We have developed procedures to isolate and expand them in vitro, enabling their functional characterization. R-DC-like cells proliferate in vitro, continue to express RORγt, and differentiate into CD1c$^+$ DC2-like cells. They stimulate the proliferation of allogeneic T cells. The identification of human R-DC-like cells with proliferative potential and plasticity toward CD1c$^+$ DC2-like cells will prompt further investigation into their impact on immune homeostasis, inflammation, and autoimmunity.

dendritic cells | innate lymphoid cells | human | retinoid-related orphan receptor gamma t | antigen presentation

Retinoid-related orphan receptor gamma t (RORγt) is a lymphoid lineage-defining transcription factor that is essential for thymopoiesis, lymphoid organogenesis, and differentiation of T_H17 cells and group 3 innate lymphoid cells (ILC3) that provide adaptive and innate sources of IL-17 and IL-22 (1–5). Recent work has unveiled the existence of innate RORγt$^+$ MHCII$^+$ APCs (antigen-presenting cells) in the mouse intestinal mucosa and mesenteric lymph nodes, which confer tolerance to microbiota and/or self-antigens by priming intestinal regulatoryT cells early in life (6). The nature of these cells is under debate: One study identified them as Thetis cells, including AIRE$^+$ and AIRE$^-$ subsets (7); other studies defined them as AIRE$^+$ Janus cells with features of medullary thymic epithelial cells and DC (dendritic cells) (8, 9) or as MHCII$^+$ group ILC3 (9, 10). A human DC subset in blood has also been reported to express low levels of RORγt (11), but the identity of these cells remains elusive. By conducting an extensive multiomic analysis of innate RORγt$^+$ cells present in mucosal tissues, we have pinpointed a distinct human cellular subset that co-expresses RORγt and markers typical of myeloid cells. We have established procedures for identifying, isolating, expanding this cell type in culture, and demonstrated its capability to activate T cells.

Results

Identification of Two Unique RORγt$^+$ Cell Types in the Human Intestinal Mucosa. To find the human counterpart of intestinal RORγt APCs, we performed scRNAseq of CD45$^+$CD3$^-$CD19$^-$ cells isolated from the lamina propria (LP) of terminal ileum surgically resected from adult patients (12) (Fig. 1*A*). After in silico removal of *RORC*$^-$ cells, the remaining *RORC*$^+$ cells projected onto a Uniform Manifold Approximation and Projection (UMAP) clustered into 7 populations (Fig. 1*A*). All clusters expressed *IL23R*,

Significance

The immune system's role in maintaining self-tolerance and preventing autoimmunity is critical. Recent mouse studies have identified dendritic cell (DC) populations that preserve immune tolerance to intestinal microflora in the gut. These cells are characterized by the expression of the transcription factor RORγt (Retinoid-related orphan receptor gamma t). The existence of similar cells in humans remains unclear. Through comprehensive multiome analysis, we have identified a unique cell population expressing both RORγt and myeloid cell markers, which we have termed RORγt$^+$ DC-like cells. These cells exist in tissues and, when cultured in vitro, develop the ability to stimulate T cells. Our study has laid the groundwork for their identification, isolation, culture expansion, and functional assessment, offering an opportunity to gauge their impact on human health and disease.

Reviewers: F.R., Malaghan Institute of Medical Research; and J.Y., City of Hope National Medical Center.

The authors declare no competing interest.

[1]A.U.A. and S.L. contributed equally to this work.

[2]To whom correspondence may be addressed. Email: william.vermi@unibs.it or mcolonna@wustl.edu.

This article contains supporting information online at https://www.pnas.org/lookup/suppl/doi:10.1073/pnas.2318710120/-/DCSupplemental.

Published December 18, 2023.

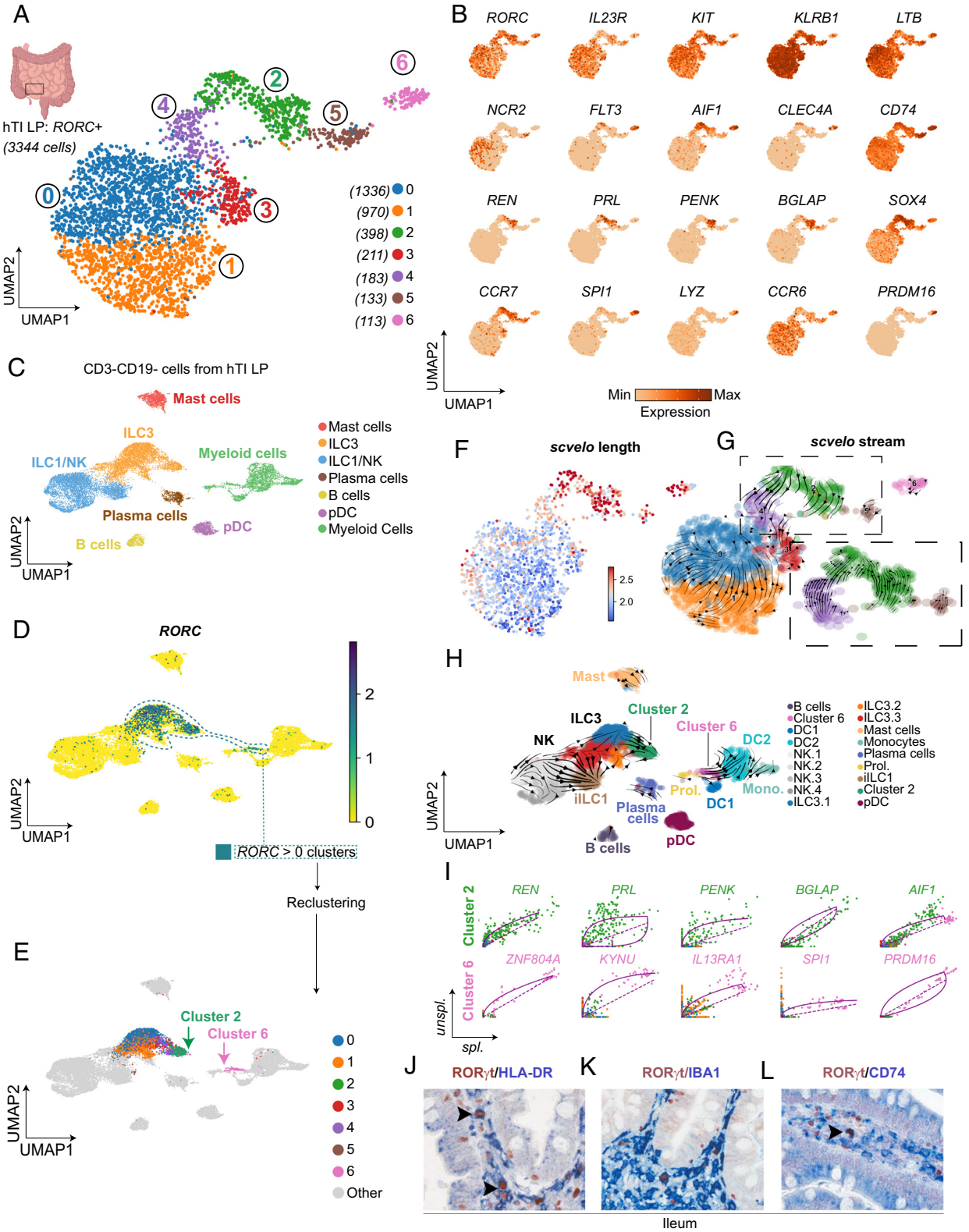

Fig. 1. scRNAseq of LP cells from the terminal ileum identifies *RORC*$^+$ cells distinct from conventional ILC3. (*A*) UMAP of *RORC*$^+$ cells from the human terminal ileum LP (n = 6 patients, total = 3,344 cells). (*B*) Scaled and normalized expression of selected genes. (*C*) UMAP of all CD3$^-$ CD19$^-$ cells sequenced from the LP of the terminal ileum (hTI LP) colored by major cell type identity (n = 17,056 cells sequenced). (*D*) Expression of *RORC* on cells on UMAP in (*C*). (*E*) Projection of cell barcodes belonging to *RORC*$^+$ clusters from *A* onto the UMAP in (*C*). Color code is matched to colors in *A*. (*F*) Computation of velocity vector length of cells displayed in *A* as calculated by recovering velocity dynamics using *scvelo*. (*G*) Velocity stream from *scvelo* (dynamic model) showing the smoothed velocity vector direction of each cell. (*H*) Velocity stream of all CD3$^-$CD19$^-$ LP cells as computed by the dynamic model of *scvelo*. (*I*) Phase portraits representing the dynamics of selected defining genes for clusters 2 and 6. The purple line represents *scvelo*'s fitted splicing dynamics. (*J*–*L*) Immunohistochemistry showing co-staining of RORγt with HLA-DR (*J*), IBA1 (*K*) and CD74 (*L*) in human ileum. iILC1 = intraepithelial ILC1.

KIT, *KLRB1* (for CD161), *CCR6,* and *LTB* (for Lymphotoxin β) (Fig. 1*B*). Clusters 0, 1, and 3 encompassed conventional ILC3, which showed variable expression of *NCR2* (encoding NKp44), markers of NF-κB activation (cluster 1), inflammatory chemokines and cytokines such as *CXCL8*, *CXCL2*, and *CSF2* (cluster 3) and *IL22* (cluster 0) (Fig. 1*B* and *SI Appendix,* Fig. S1 *A* and *B*). Clusters 2 and 6 encompassed rare cell populations (average recovery 70 to 85 cells/sample and 20 to 25 cells/sample, respectively) distinct from ILC3. They shared expression of *FLT3*, *AIF1* (for the myeloid marker IBA1), *CLEC4A*, and genes for antigen presentation, such as *CD74*, *HLA-DR, HLA-DP, HLA-DQ,* and cathepsins (Fig. 1*B* and *SI Appendix*, Fig. S1*C*). Cluster 2 uniquely expressed transcripts for hormones and soluble factors, such as renin (*REN*), prolactin (*PRL*), proenkephalin (*PENK*), and osteocalcin (*BGLAP*–bone gamma carboxy-glutamate protein) (Fig. 1*B* and *SI Appendix*, Fig. S1*A*), which are normally produced by kidney juxtaglomerular cells, pituitary gland, and osteoblasts; few cells also expressed *GNRH1* (for gonadotropin-releasing hormone) (*SI Appendix*, Fig. S1*B*). Cluster 2 also showed a distinctive array of transcription factors, including *SOX4, HOXA9*, *MEIS1,* and *RUNX1* (Fig. 1*B* and *SI Appendix*, Fig. S1 *A* and *B*), which are involved in hematopoietic stem cells renewal (13), high levels of *SPINK2* and *RASD1*, as well as *TNFSF11* (for RANKL), and *CCR7* (Fig. 1*B* and *SI Appendix,* Fig. S1 *A* and *B*). Cluster 6 segregated apart from the other clusters expressing *RORC* on the UMAP (Fig. 1*A*) due to the unique expression of myeloid-related markers, including *SPI1*, *LYZ*, and *CD300A* (Fig. 1*B* and *SI Appendix*, Fig. S1*B*). Additional unique markers of cluster 6 included: the transcription factors *PRDM16*, which is often translocated in acute myeloblastic leukemia (14) and *FOXP2* (Fig. 1*B* and *SI Appendix*, Fig. S1*B*); the polymeric immunoglobulin receptor *PIGR*; the decoy receptor for IL-22 (*IL22RA2*) that modulates IL-22 activity (15); and *CD4* (*SI Appendix*, Fig. S1 *B* and *D*). Clusters 4 and 5 could not be annotated due to lack of unique lineage markers. When we projected all LP cell types together, cluster 2 positioned close to ILC3, while cluster 6 segregated with myeloid cells on the UMAP (Fig. 1 *C–E* and *SI Appendix*, Fig. S1*D*), further supporting the distinct nature of these cell populations.

To gain further insights into the relationship of cluster 2 and cluster 6 with other *RORC*$^+$ cells, we performed RNA velocity. Clusters 2 and 6 showed the greatest vector length (Fig. 1*F*), suggesting a fast rate of differentiation. Cluster 2 showed clear directionality toward ILC3; cluster 6 cycled in an independent direction (Fig. 1*G*). When RNA velocity was performed in the context of all LP cells (defined in *SI Appendix*, Fig. S1*D*), cluster 6 pointed toward CD1c$^+$ DC2 (Fig. 1*H*). The most influential genes contributing to RNA velocity dynamics were the core signature transcripts of each cluster: hormone transcripts for cluster 2; *ZNF804A*, *SPI1, KYNU*, *IL13RA1, and PRDM16* for cluster 6; *AIF1* for both (Fig. 1*I*). RNA velocity also revealed that dynamic genes for clusters 2 and 6 were mostly unspliced, suggesting high transcriptional induction (Fig. 1*I*). Pearson analysis confirmed that cluster 6 displayed the highest transcriptional correlation to DC2, DC1 and monocytes across all sequenced CD45$^+$CD3$^-$CD19$^-$ cells (*SI Appendix*, Fig. S1*E*). Notably, cluster 6-like cells were present in other scRNAseq databases from the intestinal mucosa and from other mucosae. We identified cluster 6-like cells in the terminal ileum atlas of Crohn's disease and healthy patients (16) as a subset named cluster 4 positioned between non-proliferating and proliferating DC2 (*SI Appendix*, Fig. S2 *A–D*). Moreover, signature transfer from cluster 6 cells to scRNAseq data from biopsies of nasal-associated lymphoid tissues of COVID-19 patients and healthy controls (17) identified similar cells expressing *RORC*, *PRDM16* and *FOXP2* as a rare subset of DC located between DC2 and *LAMP3*$^+$*CCL19*$^+$*CCR7*$^+$ mature DC (mDC) (*SI Appendix*, Fig. S2 *E–I*). Conversely, we did not detect cluster 6-like cells in a scRNAseq database encompassing ~99,000 of human peripheral blood cells (18) (*SI Appendix*, Fig. S3 *A–D*).

To spatially locate cluster 2 and cluster 6 cells in the intestinal mucosa, we resorted to immunohistochemistry and RNAscope. Intestinal RORγt$^+$CD3$^-$ cells encompassed rare cells with a relatively large non-lymphocytic morphology that co-expressed markers of clusters 2 and 6, such as HLA-DR, IBA1, and CD74 (Fig. 1 *J–L*). Serial sections of the small intestine showed rare cluster 2-like cells co-expressing RORγt and CCR7 proteins together with *PENK* RNA in the periphery of Peyer's Patches (*SI Appendix*, Fig. S4 *A* and *B*) or at the base of the intestinal villi (*SI Appendix*, Fig. S4 *C–F*). We also noted cells co-expressing RORγt and CCR7 proteins with either *PENK*, *REN*, *PRL* RNAs (*SI Appendix*, Fig. S4 *G–O*), or with both *REN* and *PENK* RNAs (*SI Appendix*, Fig. S4 *P–R*). Cryptopatches showed cluster 6-like RORγt$^+$ cells expressing SPI1 (*SI Appendix*, Fig. S4 *S* and *T*); immunohistochemistry of serial sections identified rare cells co-expressing RORγt, IL-22BP, and CLEC4A (*SI Appendix*, Fig. S4 *U* and *V*). However, SPI1, CLEC4A, or IL22BP were not exclusively expressed in RORγt$^+$ cells, as many other cells, including DC2, expressed these proteins.

To further understand the nature of clusters 2 and 6, we performed a linear regression–based cell-type prediction analysis of all LP *RORC*$^+$ clusters to see how they matched to immune cells reported in the Cross-Tissue Immune Cell Atlas (19), the gut atlas (20), and the thymic atlas (21) using the recently developed tool Celltypist (19). Cluster 2 mostly mapped to ILC, specifically ILC3 (*SI Appendix*, Fig. S5 *A–H*), and in part to lymphocyte progenitors, such as common lymphoid and early T-cell progenitors (*SI Appendix*, Fig. S5 *C–H*). Conversely, cluster 6 exclusively mapped to DC, particularly DC2 (*SI Appendix*, Fig. S5 *A–H*). Because mouse RORγt$^+$ APCs were found early in life (6), we matched our entire LP scRNAseq dataset to the fetal tissue atlas (22): Cluster 2 was annotated as "Lympho-myeloid primed progenitor/ILC3", while cluster 6 was classified as "DC progenitor" (*SI Appendix*, Fig. S5*I*). Further supporting that cluster 2 was related to ILC3 progenitors, flow cytometry showed that LP CD34$^+$ progenitors included a subset of RORγt$^+$CCR7$^+$CLEC4A$^+$ HLA-DR$^+$ cells (*SI Appendix*, Fig. S5*J*), which were reminiscent of the precursors shown to generate mature ILC3 upon in vitro culture with IL-7, SCF, and IL-15 (23, 24). Celltypist prediction analysis using a recently published dataset of mouse Thetis cells (7) and cosine similarity analysis to mouse Immgen data (25) showed that cluster 2 mapped to lymphoid-inducer cells and NCR$^+$ ILC3, while cluster 6 mapped to Thetis cells and DC (*SI Appendix,* Fig. S5 *K* and *L*). Collectively, these analyses identify two rare cell populations within CD3$^-$CD19$^-$ RORγt$^+$ cells of the human intestinal LP: One population (cluster 2) corresponds to a CD34$^+$ ILC3 progenitor, thereafter referred to as ILC3p; another population (cluster 6) is related to, but distinct from, DC2 and fetal DC progenitors, thereafter referred to as RORγt$^+$ DC-like cells (R-DC-like). Both cell types express transcripts associated with antigen presentation and are distinct from conventional mature ILC3.

Isolation and Characterization of R-DC-Like Cells from Human Tonsils. We sought to obtain an in-depth characterization of R-DC-like by paired scRNAseq/scATACseq. However, the limited amount of intestinal tissue available from surgical resections restricted this purpose. Thus, we chose to identify and isolate R-DC-like in tonsil, a readily available and abundant source of mucosal-associated immune cells. Since LP cluster 6 cells had features of DC progenitors and DC, but also shared a few features with ILC3, we chose to separately enrich DC1 (HLA-DR$^+$CD4$^+$CD1c$^-$), DC2

(HLA-DR$^+$CD4$^+$CD1c$^+$), NCR2$^+$ILC (NKp44$^+$) and CD34$^+$ progenitors from tonsil and mix them in approximate 1:1:1:1 ratio to maintain equal representation (Fig. 2 *A* and *B*). The resulting pool was analyzed by paired scRNA/scATACseq. After excluding a few contaminating endothelial cells, fibroblasts, mast cells, and B cells, the RNA UMAP identified R-DC-like in a cluster distinct from 8 other clusters encompassing CD34$^+$ progenitors, ILC3p, *NCR2*$^+$ ILC3, NK cells, DC1, DC2, and *LAMP3*^{high}*CCR7*^{high} mDC (Fig. 2*C*). However, the R-DC-like identified were in insufficient numbers for in-depth characterization (139 cells out of 22,374 cells sequenced). Thus, we refined our sorting strategy by including Lin$^-$HLA-DR$^+$CD4$^-$CD1c$^-$ cells which were not considered in the first gating strategy, while most of the NKp44$^+$ (*NCR2*$^+$) ILC3 were excluded (Fig. 2 *D* and *E*). Paired scRNA/scATACseq of this pool of cells showed a 20-fold increase in the abundance of R-DC-like, suggesting that these cells are enriched

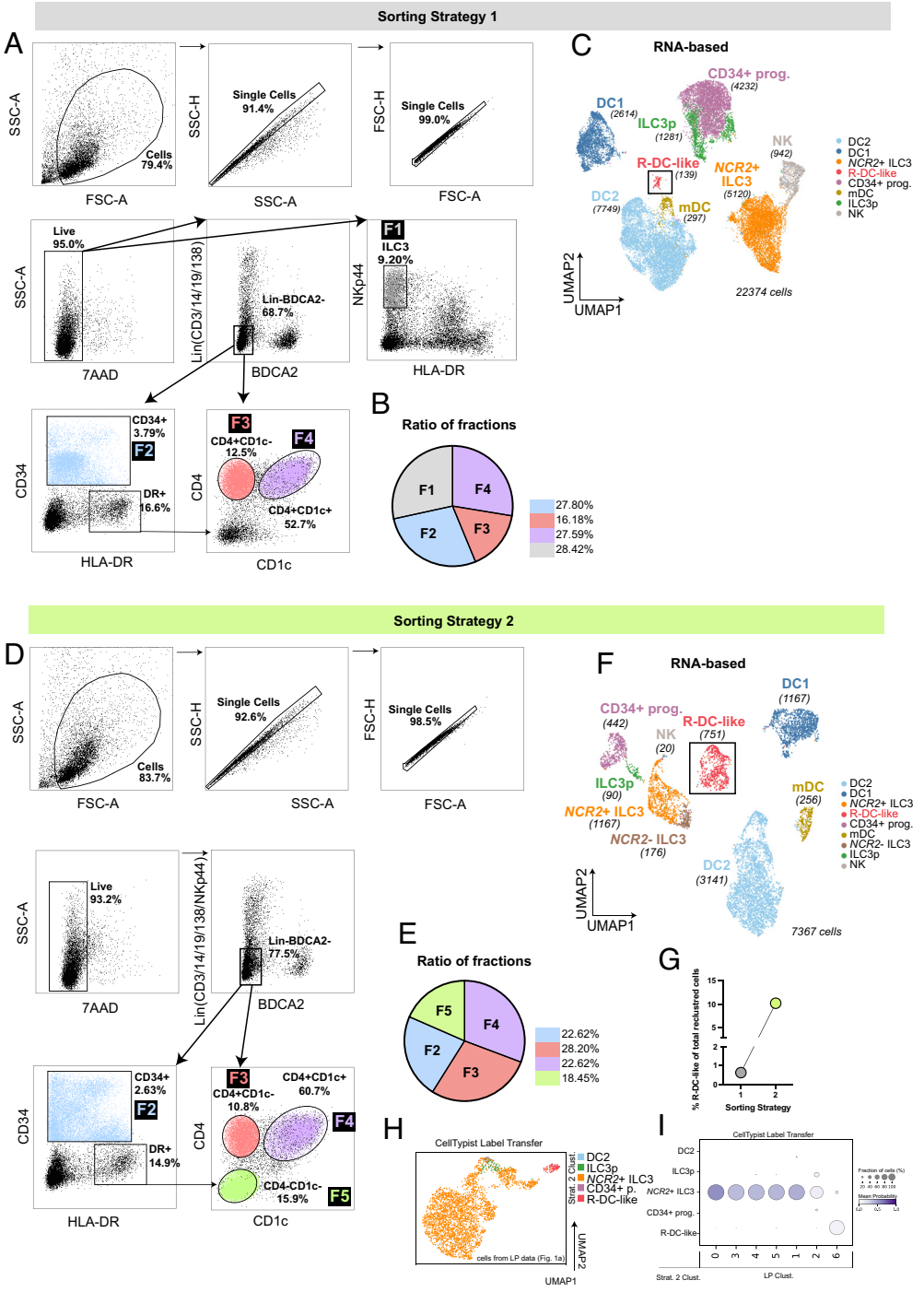

Fig. 2. Sorting strategies to enrich R-DC-like. (*A*) Gating strategy corresponding to sorting strategy 1. F = fraction. (*B*) Pie chart representing the ratios in which F1-4 were mixed before sending for paired scRNA/scATACseq. (*C*) Seurat-derived RNA-based UMAP of the resulting clusters. In parenthesis is shown the number of cells in each cluster, and in the *Lower Right* is the total number of cells represented in the UMAP. (*D*) Gating strategy corresponding to sorting strategy 2. F = fraction. (*E*) Pie chart representing the ratios in which F2-5 were mixed before sending for paired scRNA/scATACseq. (*F*) Seurat-derived RNA-based UMAP of the resulting clusters. In parenthesis is shown the number of cells in each cluster, and in the *Lower Right* is the total number of cells represented in the UMAP. (*G*) Graph showing the percentages of R-DC-like recovered from strategy 1 and strategy 2 as a fraction of the total cells sequenced. (*H*) *RORC*$^+$ LP clusters from Fig. 1*A* fitted into the CellTypist-trained tonsil dataset from sorting strategy 2. Each cell is colored by the "best match" label from the tonsil dataset. (*I*) Dot plot representing the quantification of the results in *H*.

in the Lin$^-$HLA-DR$^+$CD4$^-$ fraction (Fig. 2 *F* and *G*). CellTypist prediction analysis corroborated that the tonsil R-DC-like cluster corresponded to LP cluster 6 cells (Fig. 2 *H* and *I*).

The RNA UMAP of all cells enriched from tonsils identified R-DC-like as a unique cluster that exhibited more transcriptional similarity to DC1, DC2, and mDC than to ILC3 and progenitors (Fig. 3*A* and *SI Appendix*, Fig. S6*A*). A Sashimi plot reconstruction demonstrated that splicing of the RORC gene initiated from the RORγt promoter, indicating that R-DC-like, like ILC3, express RORγt rather than RORγ (Fig. 3*B*). In addition to *RORC,* R-DC-like expressed the transcription factors *PRDM16, SPI1, ZBTB46, FOXP2*, and *RUNX3* but not *RORA* (Fig. 3*C* and *SI Appendix*, Fig. S6*B*); R-DC-like expressed transcripts for the cell surface molecules *FLT3, KIT, CLEC4A, PIGR, CCR6, ITGAE,* and *IL23R* (Fig. 3*C* and *SI Appendix,* Fig. S6*C*). Additional R-DC-like markers included *AIF1, LYZ,* and *IL22RA2* and the microbial sensors *TLR10* and *NOD1* (Fig. 3*C* and *SI Appendix*, Fig. S6*D*). Among genes for effector molecules, R-DC-like expressed *LTB*, *CXCL13, CKLF* (for Chemokine Like Factor), and *DEFA4* (for Defensin α4) (*SI Appendix*, Fig. S6*E*). Further corroborating their uniqueness, R-DC-like lacked *AIRE* and hormonal transcripts typical of mDC and ILC3p, respectively (Fig. 3*C*). Re-clustering of R-DC-like yielded 4 distinct clusters (Fig. 3 *D* and *E*): a major population of *RORC*^{high} cells (cluster 1); a population of *RORC*^{int} cells that expressed *ZEB2*, *RUNX1*, *CLEC10A* and low levels of *CD1C* (cluster 2); a population of *RORC*^{high} proliferating cells (cluster 0) positioned between clusters 1 and 2; a minor cluster of *IL7R*$^+$ *KIT*$^+$ cells (cluster 3). RNA velocity indicated that proliferating cells generated both *RORC*^{high} and *RORC*^{int}*CD1C*^{low} cells (Fig. 3*D*). Altogether, we conclude that our gating strategy enables the identification of a substantial population of R-DC-like in tonsils that is distinct from DC2, other DC subsets, CD34$^+$ progenitors, ILC3p, and ILC3.

The sorting strategy used to identify R-DC-like provided a basis to precisely recognize them by flow cytometry (Fig. 3*F*). Within tonsil Lin$^-$CD45$^+$, we excluded CD34$^+$ cells (R1), which contained a fraction of MHCII$^+$RORγt$^+$ ILC3p. Within Lin$^-$CD45$^+$CD34$^-$ cells (R2), we excluded NKp44$^+$NKp46$^+$ (*NCR2*$^+$) ILC3 and NKp46$^+$NKp44$^-$ NK cells (R3). By further excluding NKp44$^-$ CD161$^+$ (*NCR2*$^-$) ILC3 and gating on HLA-DR$^+$ cells (R4), we identified 3 discrete subsets based on CD4 and CD1c expression. CD4$^-$CD1c$^-$ cells (R5) contained the largest percentage of RORγt$^+$ cells, some of which expressed CLEC4A. CD4$^+$CD1c$^-$ cells (R6a) included a population of CLEC4A$^+$ cells, few of which showed low expression of RORγt; these CLEC4A$^+$RORγt$^+$ R-DC-like likely corresponded to R-DC-like identified in our initial sorting strategy, while the remaining CD4$^+$CD1c$^-$ cells corresponded to DC1. CD1c$^+$ cells (R6b) mostly comprised CLEC4A$^+$RORγt$^-$ DC2. We conclude that R-DC-like are mostly contained within the HLA-DR$^+$CD4$^-$CD1c$^-$ fraction of immune cells. Given that most of R-DC-like showed *CLEC4A* and *CD4* expression in scRNAseq (Fig. 3*C* and *SI Appendix*, Fig. S6*C*) but not in flow cytometry, R-DC-like may encompass cells at different stages of transcriptional and translational maturation.

R-DC-Like Exhibit Epigenetic Features Intermediate between Those of DC and ILC3. The use of paired scRNAseq/scATACseq allowed us to interrogate the genome-wide chromatin accessibility profile from the same 7,367 high-quality cells shown in Fig. 3 (26). Dimensionality reduction was computed using Latent Semantic Indexing (LSI), and the result was projected on a two-dimensional UMAP space using ArchR (26). R-DC-like represented a unique cluster of cells (Fig. 4*A*) with a distinct chromatin accessibility profile that partially overlapped with that of *NCR2*$^+$ ILC3 (Fig. 4*B*). Pearson correlation analysis of all peaks in the clusters showed that R-DC-like had the greater overlap with DC2 but, contrary to other DC subsets, also had high correlation to *NCR2*$^{+/-}$ ILC3 and progenitors (Fig. 4*C*). Motif enrichment analysis of pseudobulked clusters suggested that the open chromatin region (OCR) overlap between R-DC-like and *NCR2*$^+$ ILC3 was mostly due to transcription factors binding *RORE* elements, such as *RORC*, *RORA*, *RORB*, *NR1D1*, and *NR1D2* (Fig. 4*D*). R-DC-like OCR also showed an overlap with motifs enriched in DC2 OCR, specifically those for the AP-1-forming heterodimers *FOS* and *JUN* (Fig. 4*D*). Additionally, R-DC-like exhibited an enrichment for *SPI1* and *SPIB* motifs shared with DC1 and DC2, and an enrichment for *NFKB2* motif in common with NCR2$^+$ ILC3 and mDC (Fig. 4*D*). Top differentially enriched motifs for R-DC-like vs. NCR2$^+$ ILC3 corresponded to *SPI1*, *SPIB*, *SPIC*, *BCL11A,* and *BCL11B*, while *RUNX1/2* and *CBFB* were reduced (Fig. 4*E*). Top differentially enriched motifs for R-DC-like vs. DC2 included those for *RORC*, *RORB*, *RORA*, *NR1D1*, *NR1D2,* and *RUNX1*, while *BCL11A*, *BCL11B*, *SPI1,* and *CEBPA/B* were diminished (Fig. 4*F*). Paired RNA expression, gene activity and motif deviation scores on the UMAP space further showed that R-DC-like and DC but not ILC3 shared had high expression, gene activity and motif deviation of *SPI1*, *PRDM16* and *FOXP2*, whereas RORC was active in R-DC-like, progenitors and *NCR2*$^{+/-}$ ILC3 (Fig. 4*G*). We further examined ATAC peaks in specific loci. The RORγt—but not the RORγ—promoter was most accessible in R-DC-like, ILC3p and *NCR2*$^+$ ILC3, but not in mDC, DC2, and DC1 (Fig. 4*H*). This result corroborated the unequivocal RORγt splicing in R-DC-like (Fig. 3*B*). Examination of the *AIRE* locus revealed that the previously described conserved non-coding sequence 1 (CNS1) of *AIRE* (27) was only accessible in mDC (Fig. 4*I*), consistent with the preferential expression of AIRE in these cells (28) (Fig. 3*C*). Although R-DC-like were enriched in the HLA-DR$^+$CD4$^-$CD1c$^-$ population, the CD4 promoter was accessible in all DC subsets, including R-DC-like (Fig. 4*J*), suggesting that the *CD4* locus is poised in R-DC-like.

scATACseq-based analysis also showed a division of R-DC-like into two subsets. The *FindClusters* function of Seurat (29) applied to the LSI-based analysis iterated these two clusters as C10 and C11 (*SI Appendix*, Fig. S7*A*). Differential peak accessibility profiling suggested that C10 had more overlapping OCR with a subset of DC2, while C11 exhibited more common OCR with NCR2$^+$ ILC3 (*SI Appendix*, Fig. S7*B*). Genes that were found to be more highly expressed in C10 compared to C11 included *NFKB1*, *CD83*, *FOS,* and *JUN*. In contrast, C11 displayed higher expression of *CASS4*, *SYK,* and *CIITA* (*SI Appendix*, Fig. S7*C*). Differential motif enrichment analysis revealed that both C10 and C11 had enrichment in RORE-containing motifs and corroborated the enrichment of C10 in motifs for the AP1 family members *JUN* and *FOS* and NFKB-related transcription factors (*SI Appendix*, Fig. S7 *D* and *E*). Altogether, scATACseq corroborated that R-DC-like, while sharing RORγt expression, activity, and binding with ILC3, also exhibit DC2-like epigenetic features, particularly in the C10 subcluster.

R-DC-Like Cultured In Vitro Stimulate T Cells. With the goal of testing R-DC-like functions, we developed a procedure to culture and expand them in vitro. We sorted tonsil Lin$^-$HLA-DR$^+$CD4$^-$ cells, which contain most of R-DC-like based on scRNAseq and flow cytometry data; cells were cultured in medium containing GM-CSF, Flt3L, and SCF and analyzed between day 8 and 15 (Fig. 5*A*). During this time frame, the number of cells expanded approximately fourfold (Fig. 5*B*). The nature of expanded cells was defined by scRNAseq. Projection of cells onto a UMAP showed 2 main clusters of cells that expressed variable levels of *RORC, CCR6,* and *IL23R* (Fig. 5 *C–F*). *RORC*^{high}*PRDM16*$^+$ R-DC-like represented approximately 50 to 65% of the culture output (Fig. 5*D*); *RORC*^{int}*CD1C*$^+$ cells

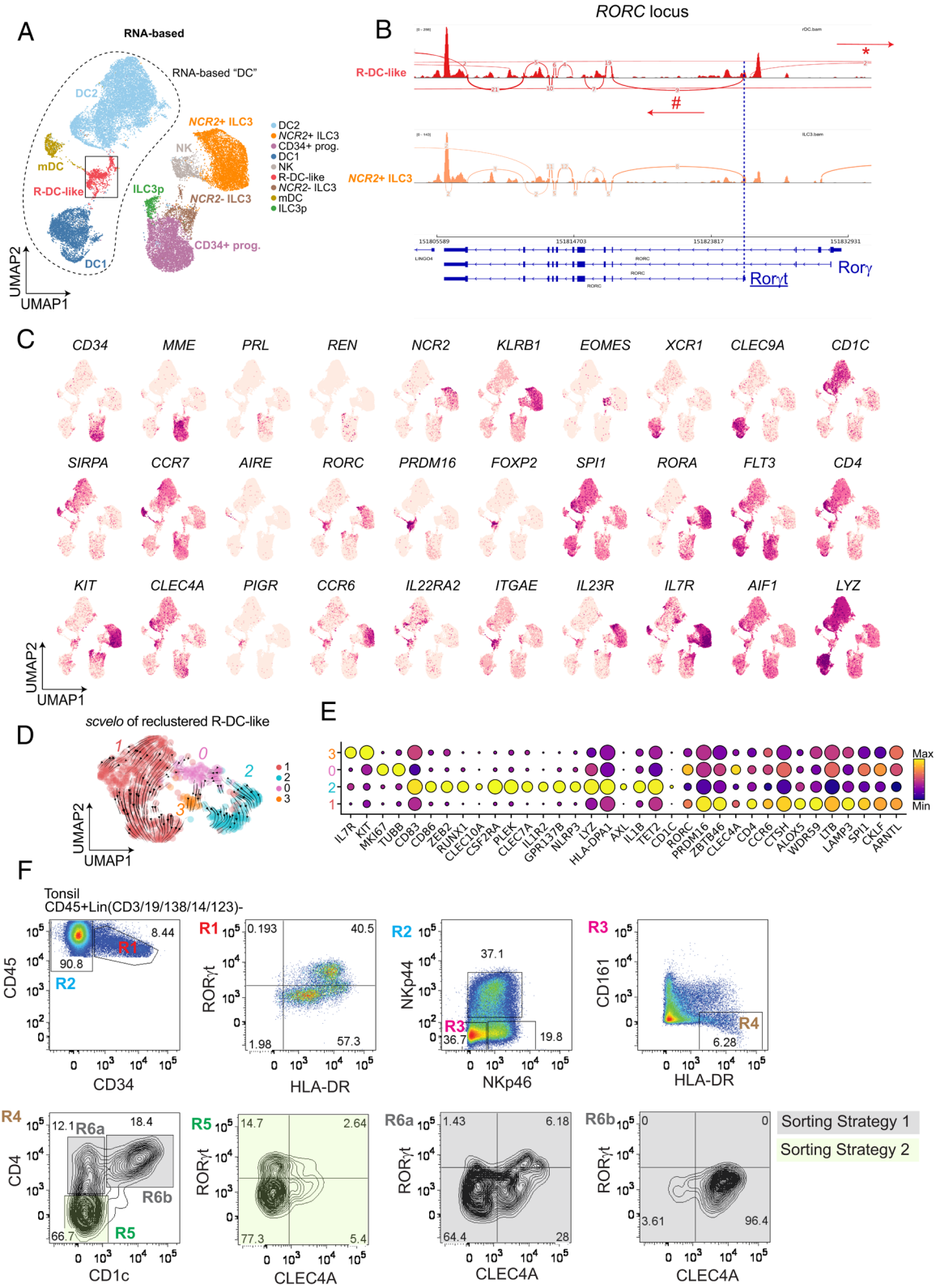

Fig. 3. scRNAseq of R-DC-like, DC1, DC2, ILC3, and CD34$^+$ cells indicates that R-DC-like are a unique cell type. (*A*) UMAP representing scRNAseq-based Seurat analysis of DC, ILC3, NK, and CD34$^+$ cells from tonsil cells (total = 29,064 cells). ILC3p = ILC3 progenitors, mDC= mature DC, R-DC-like = RORγt-expressing DC-like. (*B*) Sashimi plot reconstruction on the *RORC* locus of filtered bam files of reads belonging to cells in the R-DC-like (red) and NCR2$^+$ ILC3 (orange) clusters. Connecting lines represent intra-exonic splicing events. The discontinuous dark blue vertical line indicates the start of the RORγt promoter. (*C*) Gene expression plots of selected genes for each cluster represented on the UMAP space from *A*. (*D*) *Scvelo*-computed velocity stream of R-DC-like from *A* after re-clustering and re-processing. Colors indicate the main differentiation routes. (*E*) Dot plot of selected genes that discriminate clusters 0, 1, 2, and 3. (*F*) Flow cytometry plots of tonsil cells gated as live, singlets, CD45$^+$, Lin$^-$ (CD3/19/138/14/123). Gate order is displayed by R followed by a number. Sorting strategy colors and names refer to that of Fig. 2. One donor representative of 4 is shown.

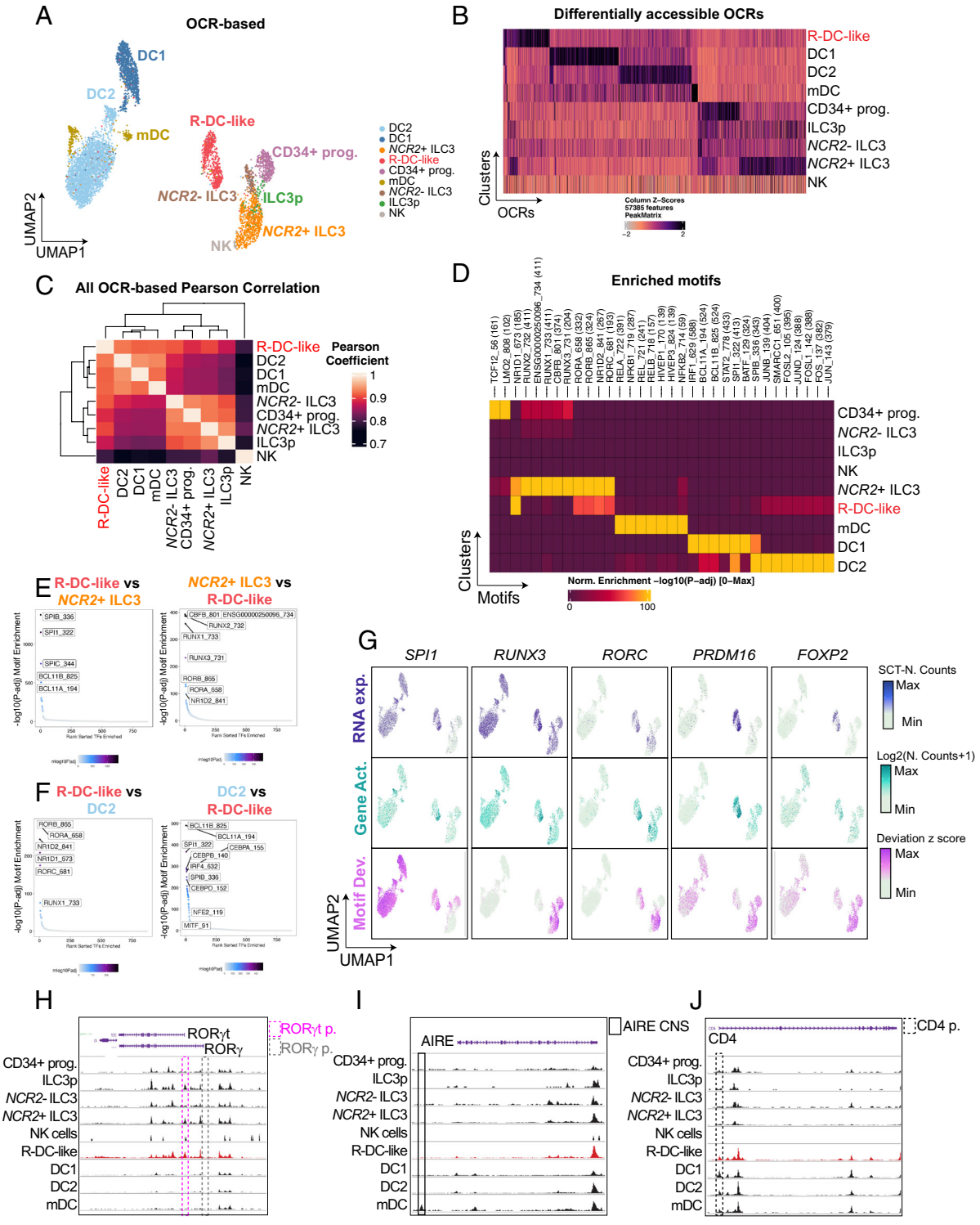

Fig. 4. scATACseq analysis indicates that R-DC-like are a unique cell type having a mixed epigenetic landscape between ILC3 and DC2. (*A*) OCR-based UMAP of tonsil cells from sorting strategy 2 using Latent Systematic Indexing-based dimensionality reduction (n = 7,367 cells). Color code matches color code in Fig. 2*A*. (*B*) Heatmap representing the z score of each peak that was differentially accessible (FDR <= 0.1 and Log2FC >= 0.5) in each pseudobulked cluster. Total peaks = 57,385. (*C*) Pearson correlation of all OCR differentially expressed among clusters identified in the UMAP in *A*. (*D*) Differential transcription factor motif enrichment (FDR <= 0.1 and Log2FC >= 0.5) in each pseudobulked cluster, normalized by motif. (*E*) Differential transcription factor motif enrichment (FDR <= 0.1 and Log2FC >= 0.5) in R-DC-like vs. NCR$^+$ ILC3 (*Left*), NCR$^+$ ILC3 vs. R-DC-like (*Right*). (*F*) Differential transcription factor motif enrichment (FDR <= 0.1 and Log2FC >= 0.5) in R-DC-like vs. DC2 (*Left*) and DC2 vs. R-DC-like (*Right*). (*G*) UMAPs of paired RNA expression (*Top* row), gene activity (*Middle* row), and motif deviation (*Bottom* row) of key transcription factors. (*H–J*) WashU Epigenome Browser-generated tracks of pseudobulked clusters from *A* on the *RORC* locus (*H*), the AIRE locus (*I*), and the CD4 locus (*J*). Discontinuous line boxes represent the promoters; the solid line box represents the CNS in the *AIRE* locus.

represented 30 to 35% of the cells; both subsets contained a fraction of *MKI67*$^+$ proliferating cells. Expression of *PIGR* and *CLEC10A* were unique to *RORC*^{high}*PRDM16*$^+$ R-DC-like and *RORC*^{int}*CD1C*$^+$ R-DC-like respectively, whereas *CLEC4A* was expressed in both (Fig. 5 *E* and *F*). CD14+ cells, AIRE+mDC and ILC3 represented minor populations (less than 10% of cultured cells in total) (Fig. 5 *C* and *D*). A Sashimi reconstruction of pseudobulked reads of R-DC-like showed that RORγt was the only isoform of *RORC* expressed

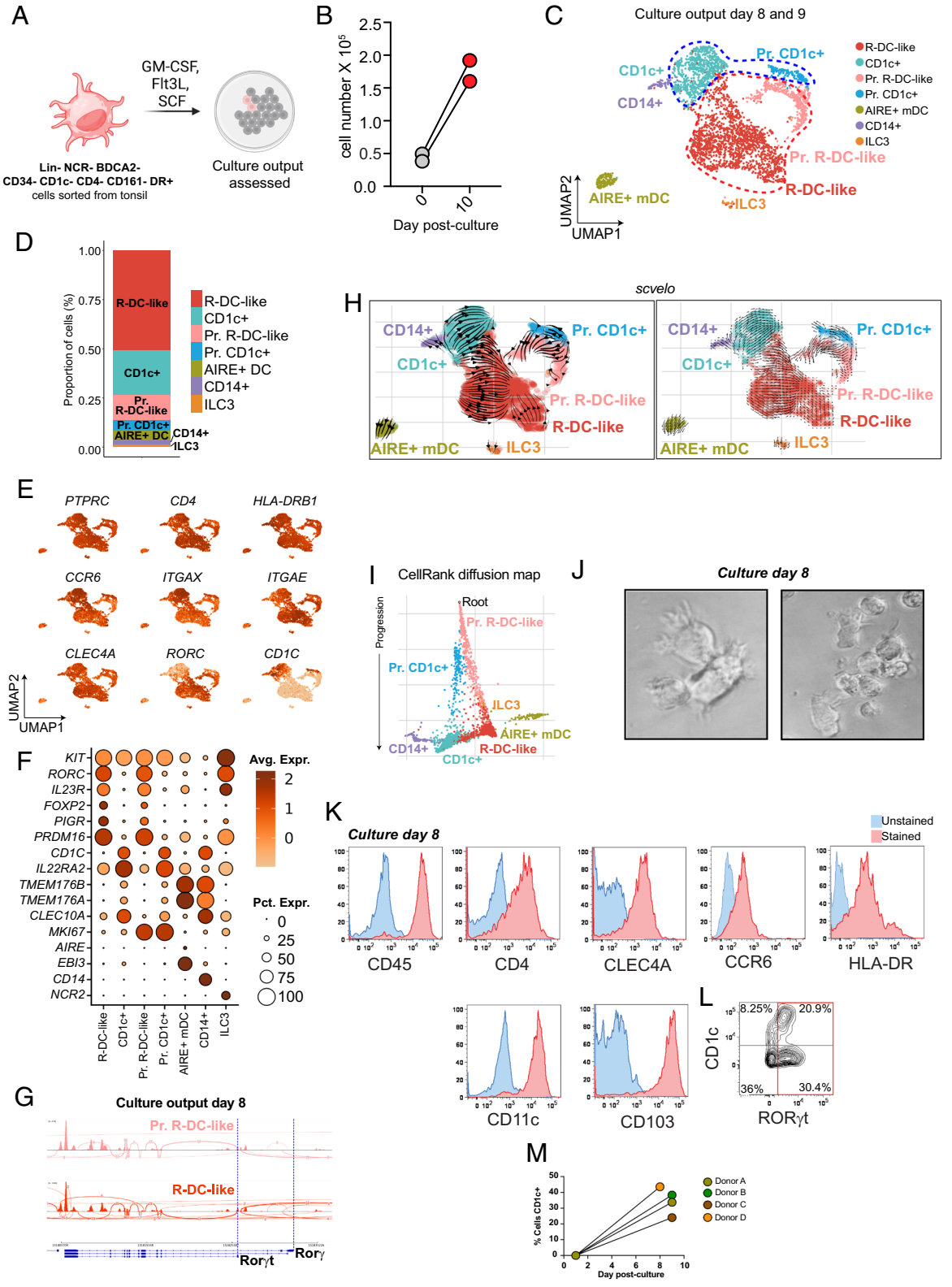

Fig. 5. In vitro cultured R-DC-like replenish themselves and generate DC2-like cells. (*A*) Schematic representation of in vitro culture conditions. (*B*) Cell numbers at day 10 after in vitro culture. (*C*) UMAP of scRNAseq of cultured cells showing the presence of four major clusters. Cells were pooled from two donors (n = 3,291 cells sequenced) and clusters were represented in each donor (Pr. = Proliferating). (*D*) Bar plot representing the contribution of each cell type to the total culture output, displayed as a per-one ratio. (*E*) Gene expression plots of selected genes. (*F*) Dot plots of indicated marker genes in each cluster. (*G*) Sashimi plot reconstruction of the filtered bam files of reads belonging to either proliferating (Pr.) R-DC-like (pink) or non-proliferating R-DC-like (red) cells on the *RORC* locus. (*H*) *Scvelo*-computed velocity stream (*Left*) and grid (*Right*) of cells from UMAP in *C*. (*I*) *CellRank* diffusion map generated by automatically identifying a "root" cell and plotting the trajectory. (*J*) Representative light-microscopy pictures of cells at day 8 of culture. Images are representative of 5 separate cultures. (*K*) Flow cytometric analysis of selected markers at day 8 of culture. Blue = negative control, red = staining. Staining is representative of 4 separate cultures. (*L*) Co-staining of CD1c and RORγt in cultured cells. Staining is representative of 3 separate cultures. (*M*) Percentage of cells positive for CD1c after 7 to 9 d of culture from four independent donors.

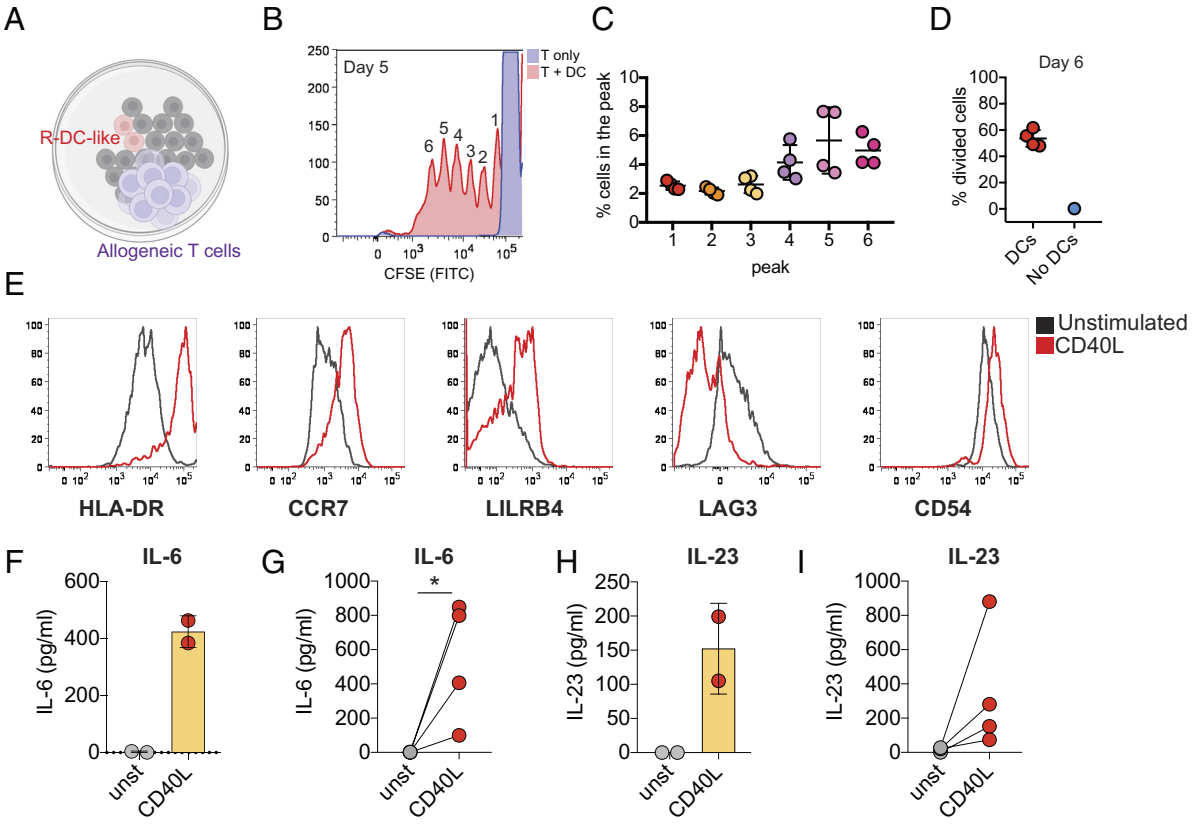

Fig. 6. In vitro generated R-DC-like induce proliferation of allogeneic T cells and upregulate HLA-DR and CCR7. (*A*) Schematic of experimental setup. (*B*) Representative histogram depicting CFSE proliferation peaks at day 5 of co-culture. One co-culture representative of 4 is shown. (*C*) Percentages of cells in each proliferating peak from panel (*B*) at day 5 of co-culture. (*D*) Percentages of CFSE$^-$ CD4$^+$ allogeneic T cells at day 6 of co-culture. Four separate R-DC-like cultures were tested. (*E*) Upregulation of HLA-DR, CCR7, LILRB4, and CD54 and downregulation of LAG3 in cultured R-DC-like upon stimulation with CD40L-expressing cells. One representative of two in vitro cultures is shown. (*F–I*) Production of IL-6 and IL-23 by in vitro cultured R-DC-like stimulated with CD40L-expressing cells. (*F* and *H*) One representative donor of four is shown. (*G* and *I*) Data from four individual R-DC-like cultures are shown.

in cultured cells (Fig. 5*G*). RNA velocity analysis indicated that *RORC*^{high} R-DC-like and *RORC*^{int}*CD1C*$^+$ R-DC-like derived from their cognate *MKI67*$^+$ proliferating subsets (Fig. 5*H*). To further estimate the most likely developmental trajectory of cultured cells, we computed a diffusion map using the CellRank package based on RNA velocity (Fig. 5*I*). This analysis predicted that the "root cell" belonged to the proliferating R-DC-like cluster, which then took two paths; one toward non proliferating *RORC*^{high} R-DC-like; another toward proliferating *RORC*^{int}*CD1C*$^+$ R-DC-like, which generated non proliferating *CD1c*$^+$ R-DC-like (Fig. 5*I*). These data recapitulated those observed in the re-clustering of primary cells isolated ex vivo (Fig. 3*D*), which showed that *RORC*^{high} and *RORC*^{int}*CD1C*^{low} cells originated from a common proliferating precursor. The yield of R-DC-like obtained by culturing HLA-DR$^+$CD4$^-$CD1c$^-$ cells was remarkably superior to that obtained by culturing other potential progenitors, such as CD34$^+$ progenitors, on OP9-Delta-like 1 feeder cells with SCF, Flt3-L, and GM-CSF or IL-7 (*SI Appendix*, Fig. S8*A*). In these culture conditions, despite robust generation of DC2, DC1 and mDC, among other cell types, R-DC-like were rare (*SI Appendix*, Fig. S8 *B–E*). Nevertheless, the few R-DC-like derived from CD34$^+$ progenitors clustered with DC2, supporting similar transcriptional features between these two cell types (*SI Appendix*, Fig. S8 *F* and *G*).

Light microscopy of R-DC-like cultured from Lin$^-$HLA-DR$^+$CD4$^-$ showed a DC-like morphology in most of the cells (Fig. 5*J*). Flow cytometry analysis showed strong expression of CD45, CD4, CD11c, CD103, CLEC4A, CCR6, and intermediate expression of HLA-DR (Fig. 5*K*). Staining for CD1c and RORγt revealed that the RORγt protein was expressed in 50 to 70% of the cultured cells, with higher levels observed in CD1c$^-$ cells compared to CD1c$^+$ cells, consistent with the scRNAseq data (Fig. 5*L*). Notably, although lacking in sorted R-DC-like prior to culture, CD4, CD1c, and CLEC4A proteins became detectable after culture, suggesting that R-DC-like further differentiate in vitro into DC2-like cells. CD1c$^+$ DC2-like cells were present in all the cultures at day 8 to 9 in variable percentages between 20 to 45% (Fig. 5*M*).

To test whether cultured R-DC-like stimulate T cells, we purified CD4$^+$ T cells from peripheral blood of unrelated donors, labeled them with CFSE, and cocultured them with R-DC-like. Assessment of T cell proliferation peaks at day 5 showed that about 20 to 25% of T cells had proliferated, and these percentages reached an average of 60% at day 6 (Fig. 6 *A–D*). We also examined whether R-DC-like cells are responsive to CD40 ligation, a well-established stimulus for inducing DC maturation. Incubating R-DC-like cells with CD40L-expressing cells led to the upregulation of HLA-DR, CCR7, LILRB4, and CD54, along with the downregulation of the R-DC-like marker, LAG3 (Fig. 6*E*). Furthermore, activated R-DC-like cells secreted IL-6 and small amounts of IL-23 (Fig. 6 *F–I*). In conclusion, R-DC-like cells exhibit some characteristics of professional APCs.

Discussion

We have identified R-DC-like as a distinct human cell type expressing MHCII and RORγt, which exhibit dual characteristics of DC2 and ILC3. These cells are found in mucosae, such as intestinal and

nasal mucosa, and mucosal-associated lymphoid tissues, such as tonsils. In contrast to a recent study (11), no RORγt DC were detected in the blood. R-DC-like encompass two subsets, RORγt^{high}PRDM16^{+} and RORγt^{int}CD1C^{+} DC2-like. The identification of R-DC-like as a distinct subset may have been overlooked due to their rarity or because they express markers of both DC and ILC3, possibly leading them to be considered cell doublets. scRNAseq and scATACseq analyses demonstrated that R-DC-like are distinct from known DC lineages such as DC1, DC2, and mature AIRE^{+} DC. Since R-DC-like are capable of proliferating, they may represent precursor cells that can further differentiate into known subsets of DC, such as DC2, under the influence of the tissue microenvironment or danger signals. Our paired scRNA/ATACseq also identified transcription factors, in addition to RORγt, which may underpin R-DC-like differentiation, such as SPI1 and PRDM16. R-DC-like were also distinct from another RORγt^{+} rare cell subset present in mucosal tissues, which corresponds to CD34^{+} ILC3p that express HLA-DR and hormonal transcripts. Whether CD34^{+} ILC3p present hormonal peptides via MHCII for tolerance or whether the hormonal peptides have other functions remains to be defined. We have defined strategies to selectively enrich primary R-DC-like from tonsils in numbers sufficient for their characterization and outlined culture conditions for expanding them in vitro while maintaining their primary features, such as the presence of RORγt^{high} and RORγt^{int} subsets. The availability of sufficient R-DC-like numbers has enabled to demonstrate their ability to stimulate CD4^{+} T cells. Moreover, activation of R-DC-like by ligation of CD40 has shown that they acquire certain features akin to those of conventional DC, such as the upregulation of MHCII, CCR7, and the adhesion molecule CD54. Further studies will be necessary to establish whether human R-DC-like and/or ILC3p are the human counterpart of Thetis and Janus cells or other RORγt^{+}MHCII^{+}APC, such as ILC3 (30), shown to induce tolerance to microbiota antigens and self-antigens in mouse (7–10). The relationship of R-DC-like with a mouse early innate lymphoid progenitor reported to exhibit an alternative DC potential (31) should also be explored.

Materials and Methods

Preparation of Cells from Tissues, *Preparation of Cells for scRNAseq and Data Analysis*, *Matched scRNAseq and scATACseq Sample Preparation*, *scRNAseq Downstream Analysis*, *Matched scRNAseq and scATACseq Analysis*, *Histology and Cell Culture*, and all other methods can be found in *SI Appendix, Material and Methods*.

All human studies were conducted under the approval of the Institutional Review Boards of Washington University. All ileum samples were provided as surgical waste with no identifiers attached on written informed consent to the Digestive Disease Research Cores Center at Washington University.

Data, Materials, and Software Availability. The accession number for scRNAseq datasets reported in this paper is GEO: GSE247692 (32). All other study data are reported in the article and/or *SI Appendix*. The code used in the analysis of the data is available upon request to the corresponding author.

ACKNOWLEDGMENTS. We thank the Genome Technology Access Center at the McDonnell Genome Institute at Washington University for scRNAseq on the 10× platform. The center is supported by the Washington University Institute of Clinical and Translational Sciences grant UL1TR002345 from the National Center for Advancing Translational Sciences (NCATS) of the NIH. We thank E. Lantelme, D. Brinja, P. Akitani and the Pathology and Immunology Flow Cytometry Core for cell sorting. We thank the Washington University Digestive Diseases Research Core (NIDDK P30 DK052574) for support. This work was in part supported by grants U19AI142733, RO1DK132327, RO1 DK126969, RO1DK124699, RO1AI134035, and Kenneth Rainin Foundation (20220038) (to M. Colonna).

Author affiliations: [a]Department of Pathology and Immunology, Washington University School of Medicine, Saint Louis, MO 63110; [b]Department of Molecular and Translational Medicine, University of Brescia, Brescia 25125, Italy; [c]Department of Head & Neck Oncology & Surgery Otorhinolaryngology, Antoni Van Leeuwenhoek Nederlands Kanker Instituut, Amsterdam 1066, The Netherlands; [d]Department of Genetics, Washington University School of Medicine, Saint Louis, MO 63110; [e]Molecular Immunity Unit, Department of Medicine, University of Cambridge, Cambridge CB2 0QH, United Kingdom; [f]Cambridge University Hospitals National Health Service Foundation Trust, Cambridge CB2 0QQ, United Kingdom; [g]Washington University Orthopedics, Barnes Jewish Hospital, Saint Louis, MO 63110; [h]Department of Lab Diagnostics, Azienda Socio Sanitaria Territoriale Spedali Civili di Brescia, Brescia 25100, Italy; [i]Immunology Program, Broad Institute of Massachussets Institute of Technology and Harvard, Cambridge, MA 02142; [j]Center for Computational and Integrative Biology, Massachusetts General Hospital and Harvard Medical School, Boston, MA 02114; [k]Department of Molecular Biology, Massachusetts General Hospital, Boston, MA 02114; [l]Infectious Diseases Institute, The Ohio State University, Columbus, OH 43210; [m]Center for Vaccines and Immunity, Abigail Wexner Research Institute at Nationwide Children's Hospital, Columbus, OH 43205; [n]Department of Pediatrics, The Ohio State University, Columbus, OH 43210; [o]Division of Gastroenterology, Massachusetts General Hospital and Harvard Medical School, Boston, MA 02114; [p]Center for the Study of Inflammatory Bowel Disease, Massachusetts General Hospital, Boston, MA 02114; and [q]Cellular Genetics, Wellcome Sanger Institute, Cambridge CB10 1SA, United Kingdom

Author contributions: A.U.A., S.L., F.M., C.F., M.B., P.F.R., S.B., T.T., J.L.F., J.D., R.J.X., M.R.C., T.W., M. Cella, W.V., and M. Colonna designed research; A.U.A., S.L., M.M., M.B., P.F.R., S.B., T.T., J.L.F., D.M., S.Z., and M. Cella performed research; R.M.N. and M.E.P. contributed new reagents/analytic tools; A.U.A., S.L., C.F., M.L.C., N.J., K.M.N., L.K., J.D., T.W., and M. Cella analyzed data; and A.U.A., S.L., C.F., M. Cella, W.V., and M. Colonna wrote the paper.

1. Z. Sun *et al.*, Requirement for RORgamma in thymocyte survival and lymphoid organ development. *Science* **288**, 2369–2373 (2000).
2. G. Eberl, D. R. Littman, The role of the nuclear hormone receptor RORgammat in the development of lymph nodes and Peyer's patches. *Immunol. Rev.* **195**, 81–90 (2003).
3. M. Pawlak, A. W. Ho, V. K. Kuchroo, Cytokines and transcription factors in the differentiation of CD4(+) T helper cell subsets and induction of tissue inflammation and autoimmunity. *Curr. Opin. Immunol.* **67**, 57–67 (2020).
4. E. Vivier *et al.*, Innate lymphoid cells: 10 years on. *Cell* **174**, 1054–1066 (2018).
5. N. Serafini, C. A. Vosshenrich, J. P. Di Santo, Transcriptional regulation of innate lymphoid cell fate. *Nat. Rev. Immunol.* **15**, 415–428 (2015).
6. J. Abramson, J. Dobes, M. Lyu, G. F. Sonnenberg, The emerging family of RORgammat(+) antigen-presenting cells. *Nat. Rev. Immunol.*, 10.1038/s41577-023-00906-5 (2023).
7. B. Akagbosu *et al.*, Novel antigen-presenting cell imparts T(reg)-dependent tolerance to gut microbiota. *Nature* **610**, 752–760 (2022).
8. J. Wang *et al.*, Single-cell multiomics defines tolerogenic extrathymic Aire-expressing populations with unique homology to thymic epithelium. *Sci. Immunol.* **6**, eabl5053 (2021).
9. R. Kedmi *et al.*, A RORgammat(+) cell instructs gut microbiota-specific T(reg) cell differentiation. *Nature* **610**, 737–743 (2022).
10. M. Lyu *et al.*, ILC3s select microbiota-specific regulatory T cells to establish tolerance in the gut. *Nature* **610**, 744–751 (2022).
11. C. C. Brown *et al.*, Transcriptional basis of mouse and human dendritic cell heterogeneity. *Cell* **179**, 846–863.e24 (2019).
12. M. Cella *et al.*, Subsets of ILC3-ILC1-like cells generate a diversity spectrum of innate lymphoid cells in human mucosal tissues. *Nat. Immunol.* **20**, 980–991 (2019).
13. V. Calvanese *et al.*, Mapping human haematopoietic stem cells from haemogenic endothelium to birth. *Nature* **604**, 534–540 (2022).
14. F. P. Duhoux *et al.*, PRDM16 (1p36) translocations define a distinct entity of myeloid malignancies with poor prognosis but may also occur in lymphoid malignancies. *Br. J. Haematol.* **156**, 76–88 (2012).
15. S. Huber *et al.*, IL-22BP is regulated by the inflammasome and modulates tumorigenesis in the intestine. *Nature* **491**, 259–263 (2012).
16. L. Kong *et al.*, The landscape of immune dysregulation in Crohn's disease revealed through single-cell transcriptomic profiling in the ileum and colon. *Immunity* **56**, 444–458.e5 (2023).
17. M. L. Coates *et al.*, Temporal profiling of human lymphoid tissues reveals coordinated defence to viral challenge. bioRxiv [Preprint] (2023). https://www.biorxiv.org/content/10.1101/2023.09.15.558006v1 (Accessed 17 October 2023).
18. D. A. Mogilenko *et al.*, Comprehensive profiling of an aging immune system reveals clonal GZMK(+) CD8(+) T cells as conserved hallmark of inflammaging. *Immunity* **54**, 99–115 (2021).
19. C. Dominguez Conde *et al.*, Cross-tissue immune cell analysis reveals tissue-specific features in humans. *Science* **376**, eabl5197 (2022).
20. R. Elmentaite *et al.*, Cells of the human intestinal tract mapped across space and time. *Nature* **597**, 250–255 (2021).
21. J. E. Park *et al.*, A cell atlas of human thymic development defines T cell repertoire formation. *Science* **367**, eaay3224 (2020).
22. C. Suo *et al.*, Mapping the developing human immune system across organs. *Science* **376**, eabo0510 (2022).
23. D. C. Hernandez *et al.*, An in vitro platform supports generation of human innate lymphoid cells from CD34(+) hematopoietic progenitors that recapitulate ex vivo identity. *Immunity* **54**, 2417–2432.e5 (2021).
24. S. D. Scoville *et al.*, A progenitor cell expressing transcription factor RORgammat generates all human innate lymphoid cell subsets. *Immunity* **44**, 1140–1150 (2016).

25. T. S. Heng, M. W. Painter, The Immunological Genome Project: Networks of gene expression in immune cells. *Nat. Immunol.* **9**, 1091–1094 (2008).
26. J. M. Granja *et al.*, ArchR is a scalable software package for integrative single-cell chromatin accessibility analysis. *Nat. Genet.* **53**, 403–411 (2021).
27. T. N. LaFlam *et al.*, Identification of a novel cis-regulatory element essential for immune tolerance. *J. Exp. Med.* **212**, 1993–2002 (2015).
28. J. R. Fergusson *et al.*, Maturing human CD127+ CCR7+ PDL1+ dendritic cells express AIRE in the absence of tissue restricted antigens. *Front. Immunol.* **9**, 2902 (2018).
29. Y. Hao *et al.*, Integrated analysis of multimodal single-cell data. *Cell* **184**, 3573–3587.e29 (2021).
30. M. R. Hepworth *et al.*, Group 3 innate lymphoid cells mediate intestinal selection of commensal bacteria–specific CD4+ T cells. *Science* **348**, 1031–1035 (2015).
31. G. Ren *et al.*, Transcription factors TCF-1 and GATA3 are key factors for the epigenetic priming of early innate lymphoid progenitors toward distinct cell fates. *Immunity* **55**, 1402–1413 (2022).
32. A. U. Antonova *et al.*, A distinct human cell type expressing MHCII and RORγt with dual characteristics of dendritic cells and type 3 innate lymphoid cells. Gene Expression Omnibus. https://www.ncbi.nlm.nih.gov/geo/query/acc.cgi?acc=GSE247692. Deposited 14 November 2023.